Atomic scale mechanism of platinum catalyst restructuring under a pressure of reactant gas

Vaidish Sumaria,† Luan Nguyen,‡ Franklin Feng Tao,*,‡ and Philippe Sautet*,†,¶

†Department of Chemical and Biomolecular Engineering, University of California, Los Angeles, CA 90094, USA

‡Department of Chemical and Petroleum Engineering, University of Kansas, Lawrence, Kansas

¶Department of Chemistry and Biochemistry, University of California, Los Angeles, CA 90094, USA

E-mail: franklintao2017@gmail.com; sautet@ucla.edu

Abstract

Heterogeneous catalysis is key for chemical transformations. Understanding how catalyst active sites dynamically evolve at the atomic scale under reaction conditions is a prerequisite for accurate determination of catalytic mechanisms and predictably developing catalysts. We combine in-situ time-dependent observation and machine learning-accelerated first-principle atomistic simulations to uncover the mechanism of restructuring of Pt catalysts under a pressure of carbon monoxide (CO). We show that a high CO coverage at a Pt step edge triggers the formation of atomic protrusions of low-coordination Pt atoms, which then detach from the step edge to create subnano-islands on the terraces, where undercoordinated sites are stabilized by the CO adsorbates. The fast and accurate machine learning potential is key to enable the exploration of ten of thousands of configurations for the CO covered restructuring catalyst. These studies open an avenue to achieve atom-scale understanding of structural dynamics of more complex metal nanoparticle catalysts under reaction.

1 Introduction

Catalysis is central to chemical production, pollution abatement, and energy transformation. Supported metal catalysts are the workhorses of the largest current chemical processes. The notion of "active site" on the catalyst, i.e. the ensemble of surface atoms responsible for bond-breaking and forming steps on the reactants, and its structure and dynamics under reaction conditions are key for understanding the catalytic performance.[1–3] There are now clear evidences that surface sites of metal catalysts might not remain as prepared during a catalytic reaction; their structures and/or compositions evolve in the reaction conditions, under a pressure of reactants and/or products of the reaction.[4–12] For example, in reducing gas H_2 the surface region of an as-prepared Rh-Pd core-shell structured bimetallic catalyst restructured to a Pd-rich surface[13,14] while the surface of as-synthesized Pt-Cu alloy nanocubes restructured to a Pt skin layer.[15]

For a simpler case of a monometallic catalyst, tracking the surface structure of the stepped Pt(557) surface at room temperature in CO at different pressures revealed that the step edges start to restructure at a CO pressure as low as 10^{-8} Torr and that a massive reconstruction occurs at a pressure of 0.5 Torr, the surface getting homogeneously covered by nanoclusters with a size of 2.2 nm.[16] This breakup of the surface creates more under-coordinated sites. When the CO pressure is decreased to 5×10^{-8} Torr, these nanoclusters reunite back to a stepped surface with curled step edges. The reversible formation of nanoclusters shows that this restructuring is driven and maintained by the high CO pressure.[16] Density Functional Theory (DFT) calculations showed that under a model CO coverage of 1 ML a surface restructured with triangular shape arrangements is more stable than the non-reconstructed surface. At the same time, restructuring of Pt(557), Pt(100), and Pt(110) was also observed in other gases such as O_2.[17] A similar phenomenon occurs on Cu(111), Ni(557), Au(111), Au(110), Co(0001) in the presence of CO.[6,18–21] The early work by Tao et al. on Pt(557)[16] evidences the extensive reconstruction but did not explore at an atomic scale the elementary steps and mechanism of the surface transformation under a pressure of CO, which is the focus of the present work.

These earlier studies show that as-prepared surface sites could be readily transformed by

the action of the adsorbates, rendering synthetic efforts to control the initial structure of the surface somewhat meaningless. Metal sites on the "surface clusters" can have lower coordination than those at the initial terrace or step sites, which can alter the activity and selectivity of the catalytic reactions.[22–32] Therefore, exploration of how the surface of a metal catalyst is restructured at an atomic scale in a gas phase of reactant(s) is key to identify catalytic active sites, fundamentally understand the catalytic mechanisms at a molecular level, and predictably develop novel, more active, more selective, or more durable catalysts.[33,34]

Other than the studies on metal single crystal surfaces, restructuring of the surface of metal nanoparticles in reactant gas, particularly Pt nanoparticles in CO or CO and O_2 mixture was studied through in-situ TEM[35,36], in-situ IR[36], EXAFS[37], and AP-XPS[37]. For instance, the oscillatory change between faceted Pt nanoparticles and rounded Pt nanoparticles during catalysis of CO oxidation at 450°C was observed by Vendelbo et al.[35] Literature established the coupling of the increase and decrease of CO conversion with the proposed switch between the faceted nanoparticles with low-miller index surface and a rounded one with a mixture of low and high (i.e. stepped) Miller index surfaces.[35] The restructuring of the morphology of metal nanoparticles in pure CO was reported.[35] The reconstruction of (100) terraces of Pt nanoparticles to high Miller index surface was suggested with in-situ STEM and in-situ IR.[36] This observation was supported by computation of adsorption energies which found the high miller-index surfaces such as (211) and (311) with adsorbed CO is thermodynamically favorable over CO on Pt(100).[36]

Although the surface restructuring phenomenon of metal catalysts under the pressure of a reactant gas is well documented experimentally, its origin and formation mechanism is not yet understood at the atomic scale, hindering rational catalyst design.[6,16,19,21] First principle atomistic modeling could be a major approach to explore the surface restructuring phenomenon under the pressure of a gas. Nevertheless, computational studies of metal catalyst surfaces and their restructurings under high adsorbate coverage are largely limited due to four major challenges: (1) the high computational expense of exploring surface reactivity using accurate first-principles calculations on surfaces described by large unit cells, (2) the numerous combinations of adsorption configurations possible at high coverages, (3) the large space of configuration for

the metal surface restructuring under a pressure of a gas, and (4) the interdependence between the surface local structure/metallic coordination and the adsorbate coverage. Hence, to provide atomic scale insights on adsorbate-induced restructuring on catalytic systems, computational modeling requires a fast but accurate energy and force calculator to enable the exploration of a large space of configurations.

To demonstrate how the atomic-scale restructuring mechanism of a metal surface under a pressure of a reactant gas could be uncovered, we integrate in-situ scanning tunneling microscopy (STM) experiments and large-scale simulations. Computationally, the determination of the CO overlayer coverage and arrangement for each Pt structure considered here requires sampling a large number of configurations, around 13000 single-point calculations. Considering the size of unit cell required, this sampling cannot be performed directly with DFT and was critically enabled here by a fast neural network potential trained on first principle Density Functional Theory (DFT) calculations. Not only one but an ensemble of low-energy configurations exists for the CO overlayer, and each configuration of the Pt atoms and this fluxionality of the adlayer will be important for the restructuring kinetics. The approach developed here enables an unbiased statistical sampling of the CO-Pt system at a given temperature and CO pressure, i.e. a grand canonical treatment at variable CO coverage. For optimal accuracy, the low-energy ensemble of structures were recalculated using DFT, so that all energies are of DFT accuracy.

Our combination of methods shows that the Pt surface restructuring is initiated by the formation of a few atoms large protrusions along the step edges and is driven by the high CO coverage, stabilizing low coordination sites. Small Pt islands, multiply coordinated with CO molecules, analogous to polymetallic carbonyl coordination complexes, can detach from the step edge to form subnano-size islands on the Pt terraces. Our calculations revealed that small islands (<12 Pt atoms), extracted from the step edge are metastable and only subnanometer-scale islands with a size of 12-19 atoms, are stable, which matches the experimentally observed 0.5-0.8 nm nanoclusters on the Pt(111) terraces with STM. We found that the stabilizing effect due to the formation of low coordination sites that strongly bind CO competes with the destabilization arising from the perturbation of the quasihexagonal pattern of CO molecules on the

terraces. CO pressure-induced Pt atom detachment from the steps is additionally shown to be kinetically accessible. In the precursor state of the detachment, a leaving Pt atom protruding from a step edge adopts a configuration of a dicarbonyl surface complex (2CO-Pt_1), facilitating its detachment.

2 Methods

Machine Learning atomistic potential of the class of High Dimensional Neural Network Potential (HDNNP) was trained on first principle Density Functional Theory (DFT) calculations. The structural and chemical environment information of each atom is used as feature to train the potential energy surface, with both total energy and atomic forces. Deploying the Weighted Atom-centered Symmetry Functions, the Cartesian coordinates defining the atomic structure of the system are converted to translational and rotational invariant feature vectors.[38–40] The training was performed using the *n2p2* code which employs an efficient approach via multi-stream extended Kalman filtering to optimize the weights of the neural network minimizing the cost function defined by the sum of squared errors of energy and forces with a flexible parameter to adjust the importance of the two.[41] The machine learned iteratively by first constructing a preliminary HDNNP that was improved systematically and self-consistently by running NNP-based simulations to sample relevant configurations and evaluate their DFT energies to determine configurations that are not accurately described. These are then included in the training set until no further problematic structures can be identified. More details on the training of the NNP and its accuracy can be found in the supporting information.

For effective reproducibility of the work, details of the hyperparameters of the symmetry function, the weight files of the neural network, and other details of the HDNNP are included in the supporting information (Section S8). The final training set consisted of 6153 structures and generated a HDNNP with a root mean square error compared to the reference DFT calculations of 1 meV/atom for energy and 0.06 eV/Å for the atomic forces. A larger set consisting of 13379 structures was used for validation with similar errors.

First principles calculations were performed with the Vienna Ab-initio Simulation Pack-

age[42,43] using the general gradient approximation (GGA) Perdew-Burke-Erzenhof (PBE) functional.[44] Core electrons were described using the projector augmented wave method.[45,46] A k-spacing of 0.25 is used for all the calculations and the k-point grid is centered at the Γ point. A cutoff energy of 400 eV is used. A C-O bond distance based correction developed by us has been applied to correct for the known over-binding of CO from Perdew-Burke-Erzenhof (PBE) functional[44], the approach being previously validated for CO adsorption on Pt(111), Pt(100), and Pt stepped surfaces.[47,48]

Global optimization was performed using Basin Hopping Monte Carlo simulations (BHMC) with an in-house open-source code. This algorithm takes advantage of local minimization to convert the potential energy surface (PES) from a curved surface to stepped shape basins.[49] The exploration of these basins is achieved by Monte Carlo sampling through atomic displacements and the Metropolis criterion. The free energy is calculated by subtracting the reference chemical potential (which is a function of temperature and pressure) of the adsorbate from the energy of the system as shown by the following equation: ΔG = $E(nCO + slab) - E(slab) - n_{CO} \times \mu_{CO}$. Additional effects to the free energy of adsorption could arise from entropy effects, but this is not accessible in the current scope of the work. Due to the low temperature used here and to the high coverage of CO which hinders CO mobility, entropic contributions are expected to be low and should not change the qualitative picture presented. Apart from the random displacements generally used in the MC algorithm, we also utilize the "Clustering mutation algorithm" developed by us previously which has shown better acceptance ratio in the BHMC simulations.[48]

To understand the kinetics of Pt restructuring under CO pressure, we cannot use the traditional nudged elastic band method since the coverage of CO keeps changing to stabilize the island formation and motion on the terrace.[50,51] Hence to simulate the extraction of one-Pt-atom protrusion at a Pt(553) step edge, we manually move the Pt atom towards the terrace perpendicular to the step edge. At each image of this extraction process, we perform grand canonical basin hopping using the fast HDNNP to find the lowest energy configuration of CO molecules. Here we make a Born-Oppenheimer type approximation such that CO molecules are allowed to move more quickly compared to Pt (island) atoms to ensure equilibrium of the

CO molecules on the surface with the gas phase CO.

The structure of Pt surfaces in a CO environment (at different pressures) was studied using a high pressure scanning tunneling microscope (HP-STM) system. The sample was placed inside the HP-STM cell (approximately 15mL in volume) with the cell door remained open for surface checking under UHV environment. For in-situ experiment, the HP-STM cell door was closed and CO gas was flown through the cell and over the sample during STM image acquisition. The sample could be heated simultaneously by an IR laser (810 nm) irradiation on the back of the sample. The sample temperature was monitored using a K-type thermocouple spot-welded onto the back of the sample. More information about this system can be found in the literature.[52]

There are three limiting factors preventing us from obtaining STM images at atom scale or a resolution better than the images presented in this article: (i) Temperature: all STM images in Figure 1 were collected at room temperature under a pressure of CO instead of lower temperature or even cryogenic temperature which significantly helps collecting a high-resolution image. (ii) Scanning speed: as we were trying to catch the evolution of surface structure, we had to scan relatively fast, limiting the number of pixels per nm^2 and lowering the image resolution. (iii) feature of the surface morphology: the narrow terrace in terms of relatively high density of step edge requires a faster feedback loop of scanning to compensate the change of tunneling current. The faster response in z-direction sacrificed the resolution. For the same reasons, no high-resolution images were obtained in the early work as well.[16]

3 Results & Discussion

3.1 In situ imaging of restructuring at nanoscale

A sequence STM images was acquired on the same stepped region of our Pt(111) sample in CO gas at a pressure of 1.5×10^{-6} Torr (Fig. 1). The terraces are ~5-10 nm wide. A low pressure is selected to slow down the surface restructuring events so that consecutive steps of the restructuring process can be tracked. Fig. 1(a) shows the image of the surface just after the

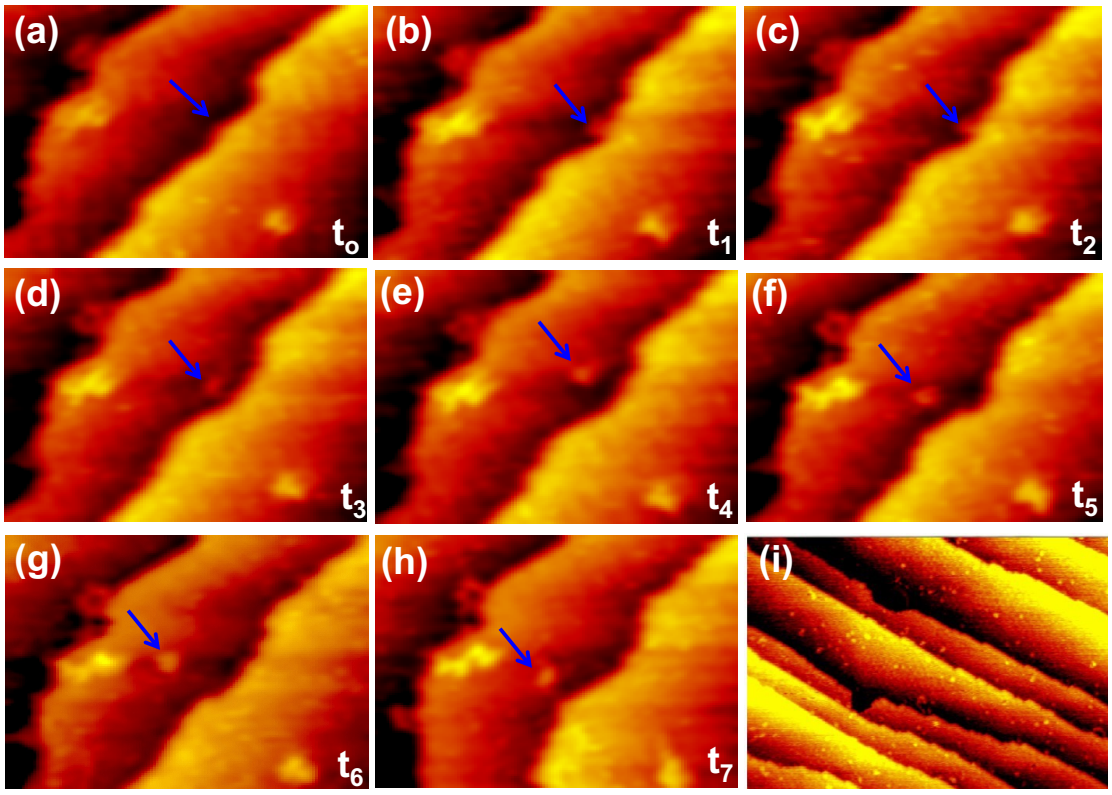

Figure 1: STM images of a Pt(111) surface at room temperature in gaseous CO. (a-h) STM images of the same region taken sequentially at different times: (a) t_0 = 0, (b) t_1 = 10, (c) t_2 = 12, (d) t_3 = 14, (e) t_4 = 16, (f) t_5 = 23, (g) t_6 = 25, (h) t_7 = 27 min after the CO pressure was brought up to 1.5 $\times 10^{-6}$ Torr at room temperature; the size of each image (a-h) is 15 nm×20 nm; the acquisition time of each image is 1-2 minutes. In (a-h), the progressive detachment of a subnanometer cluster was observed experimentally. (i) STM image under a CO pressure of 0.1 Torr; size of the image is 30 nm×40 nm; nanoclusters with a size of 0.5-0.8 nm appeared as bright spots on terraces of Pt(111).

introduction of CO. It features terraces with irregular step edges of Pt atoms. The blue arrow marks the area that evolves as a function of time. After 10 minutes (Fig. 1(b)), a subnanometer protrusion forms at the step, towards the lower terrace. This "peninsula" detaches from the step edge after 14 minutes (Fig. 1(c)), forming a subnanometer size cluster on the terrace. The cluster then diffuses on the surface, with a slight apparent increase in size (Fig. 1(e)). The size of the Pt cluster does not increase further after 16 minutes while it continuously diffuses on the terrace. The pressure of CO has a major influence on the rate of these detachments of Pt clusters from the step. No such detachment was observed during the duration of the experiment for the same sample in UHV or under a CO pressure of 5×10^{-8} Torr (Fig. S3). In contrast, at a higher pressure of 0.1 Torr, a great number of Pt nanoclusters with size of 0.5-0.8 nm were

formed on the terraces (Fig. 1(i)).

The images give important information on the surface transformation, but they do not provide an atomic scale mechanism of the restructuring. The time scale required to acquire the image is long (at least tens of seconds) preventing to record detailed time evolution. Hence, the specific atomistic structure of Pt atoms and CO molecules and the rearrangement kinetics on the surface is unknown. It is therefore mandatory to couple the experimental insight with atomistic simulations as we do here.

3.2 Grand canonical simulations of elementary restructuring processes

Various elementary steps for surface restructuring were explored using basing-hopping simulations and the trained neural network potential. A basin hopping algorithm is used to explore the potential energy surface and has shown application previously to understand CO arrangement on Pt stepped surfaces[48], fluxionality of catalytic clusters[53–56] as well as for biomolecules.[57,58] At the same time, HDNNP have been used to reduce the high computational cost of DFT simulations especially when used for global optimization problems.[53,59–62].

Two models of stepped surfaces have been considered, Pt(553) and Pt(557) (Fig S1 and S2 respectively). On Pt(553), the atoms of the step edge and their underneath atoms form triangular Pt arrangements in the counter-step (111 step) while Pt(557) gives square arrangements (100 step). The considered elementary restructuring processes are (i) step rearrangement, (ii) step atom extraction towards the lower terrace, and (iii) island formation on the terrace. One important feature is that the coverage and positions of the CO can dynamically change during each considered restructuring process. This feature has been considered by performing global optimization with basin hopping for the CO overlayer at variable CO coverage for each Pt surface structure (Section S3.3). To understand the effect of pressure, we perform the global optimization at different pressure conditions (0.0007, 0.5, and 450 Torr). Since the Gibbs free energy changes logarithmic with pressure ($G \sim k_B T ln(P/P^o)$), change in pressure from 0.0007 to 0.5 and 0.5 to 450 Torr results in a change in Gibbs free energy of ~$7k_BT \cong 0.15$ eV

(at RT). Hence with the limited accuracy of DFT calculations, these steps in pressure conditions give use a reasonable understanding of the overall effect. Since the CO diffusion barrier is low on the (111) surface of Pt and CO adsorption is not activated, we assumed that CO diffusion or addition/removal on the surface is very fast, so that the CO adlayer structure will remain in equilibrium with the gas phase upon Pt surface restructuring.

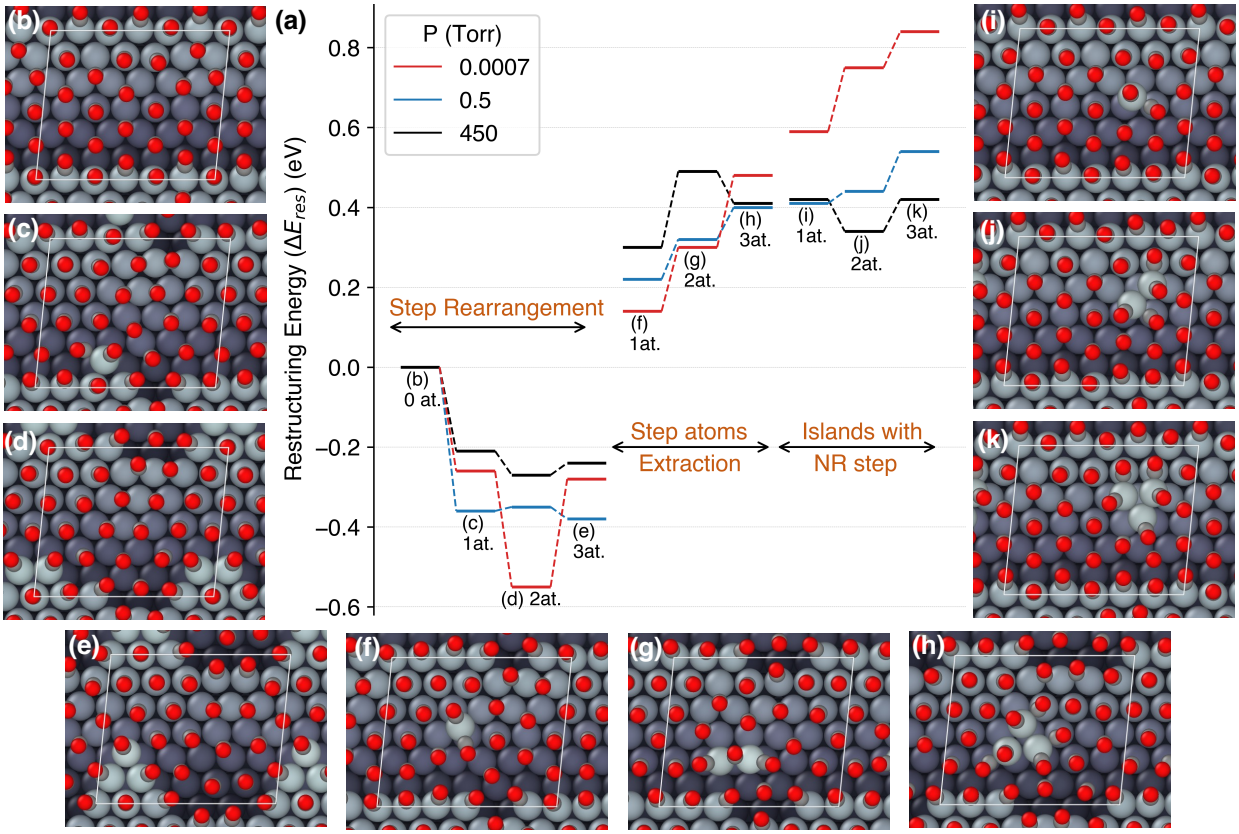

Figure 2: Simulation of elementary surface restructuring events at the Pt(557) step edge: (a) Restructuring energy under a CO pressure of 0.0007, 0.5 or 450 Torr for step rearrangement (structures b-e), step atom extraction (structures f-h) and island formation keeping the step unmodified (structures i-k). The parallelogram shown in white line marks a unit cell.

The step rearrangement process for the Pt(557) step edge is shown in Fig.2(b-d). 1, 2, or 3 atoms form a protrusion at the step edge. This process is markedly endothermic on the bare Pt(557) surface in the absence of CO adsorbates (by 0.54, 0.52, and 0.67 eV for 1, 2, and 3 atoms, respectively (Fig. S15, Table S4) since the coordination of Pt atoms is globally decreased. In contrast, under a pressure of CO, such a movement of step atoms is stabilizing by 0.2 to 0.6 eV depending on the number of Pt atoms rearranged and the pressure. Clearly, the

CO adsorbates promote the breaking of Pt-Pt bonds and the formation of low coordinated Pt atoms along the step edge. CO coverage is high, even at 0.7 mTorr pressure, with full coverage at the step edge, and 0.67 to 0.83 ML on the terrace depending on the CO pressure (Table S5). Although the amount of CO is not systematically increased following the restructuring elementary step, the presence of CO adsorbates and their rearrangement is essential for the restructuring to occur. The formation of triangular apexes induced by CO adsorption on Pt (557) as in Fig.2(e) is in good agreement with STM experiments where such "triangular" restructuring has been evidenced.[16]

3.3 Mechanism of island formation on terraces

Moving ahead, we formed 1, 2, or 3 atom islands on the terrace of the stepped surface. Two approaches are considered. The first one just extracts atoms from the step edge, forming simultaneously a small island and a kinked step. In the second approach, the step is kept unmodified, hence assuming that the island atoms thermodynamically originate from the bulk of the Pt sample. The restructuring energy (ΔE_{res}) to form these small islands under a pressure of CO is found to be positive, i.e. destabilizing, by 0.14 to 0.84 eV depending on CO pressure and the type of islands. This destabilization is much smaller than that for the surface in the absence of CO adsorbate (between 1.37 and 3.0 eV depending on the configuration; see Fig. S15), so that CO adsorption has a clear stabilizing effect on a Pt atom at low coordination, but the amplitude of the adsorption effect is not strong enough to compensate the intrinsic energy cost to form the low coordination islands. The CO coverage, here defined as the ratio of the number of CO molecules to the number of Pt atoms of an entity, such as an island or cluster, is high and depends on the size. For example, the CO coverage can be 2 for a dicarbonyl on Pt_1 (2CO-Pt_1) and 1.5 for three CO molecules on Pt_2 (3CO-Pt_2) compared to 1 for a Pt step atom of the initial surface. However, the energy stabilization contributed by the increased adsorption energy of CO is not large enough to render the structures thermodynamically stable.

Computational studies on Pt(553), another stepped surface (Fig. S1), demonstrate how the restructuring process can depend on the specific geometry of the initial step. The main effect is

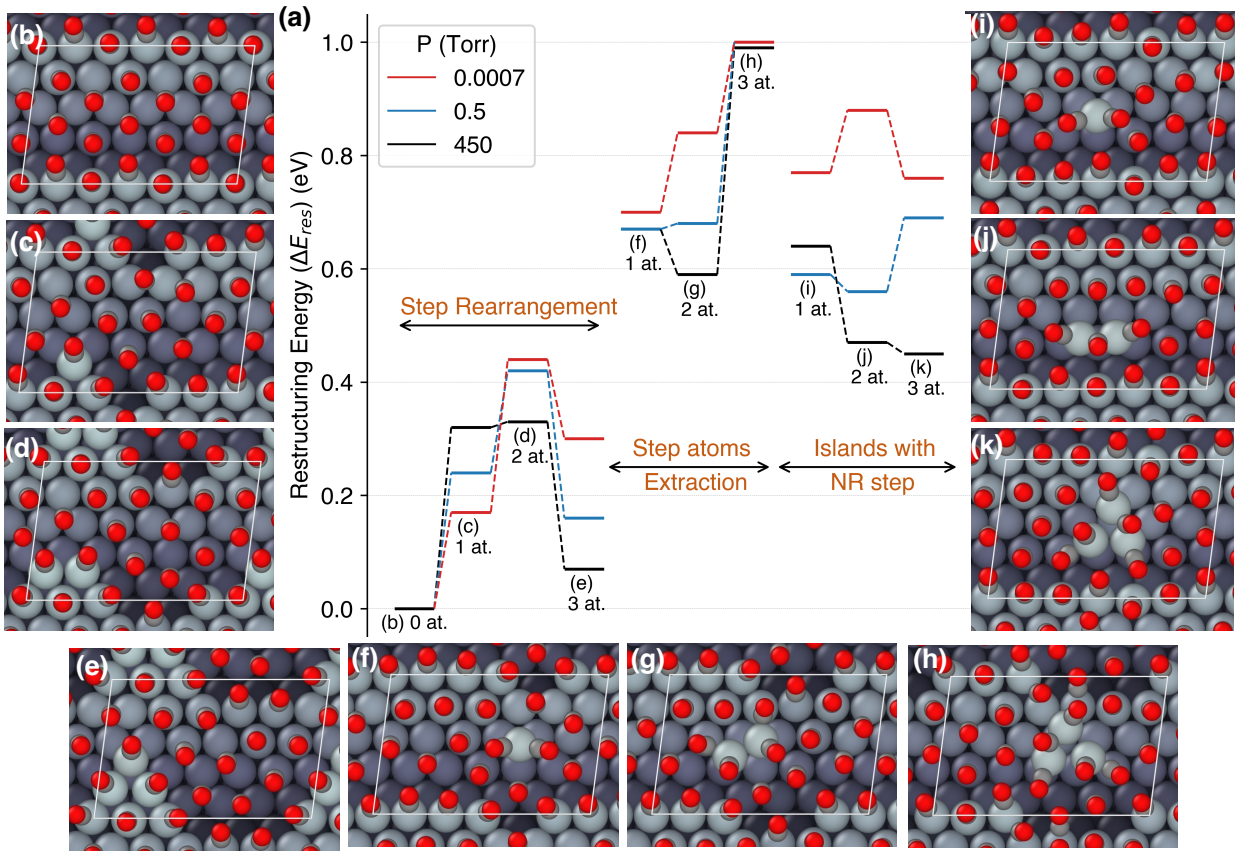

Figure 3: (a) Simulation of elementary surface restructuring events at the Pt(553) step edge: (a) Restructuring energy under a CO pressure of 0.0007, 0.5 or 450 Torr, for step rearrangement (structures b-e), step atom extraction (structures f-h) and island formation keeping the step unmodified (structures i-k).

similar, in that the stronger CO adsorption at low coordination Pt atoms. However, in contrast to Pt(557) (Fig. 2), step rearrangement events on Pt(553) are slightly endothermic by 0.1 to 0.4 eV (Fig. 3 (c, d, e)) and step atom extractions are also energetically less favored.

Since very small islands (1-3 atoms) are found to be metastable, we explored the formation of larger islands, featuring some more coordinated Pt atoms. If we suppose that an island is moved away from the unmodified step, the system can be simplified as one consisting of a terrace and supported islands as shown in Fig. 4. Here we consider the formation of monolayer islands of sizes 1, 3, 7, 10, 12, and 19 atoms on Pt(111) (1 and 3 are repeated to show the consistency with the previous model including the step). The simulations recover the previous result that islands of sizes 1 and 3 are metastable by 0.4 to 0.7 eV in the range of the considered CO pressure. Pt_7 shows similar stability. However, beyond that size, the restructuring energy

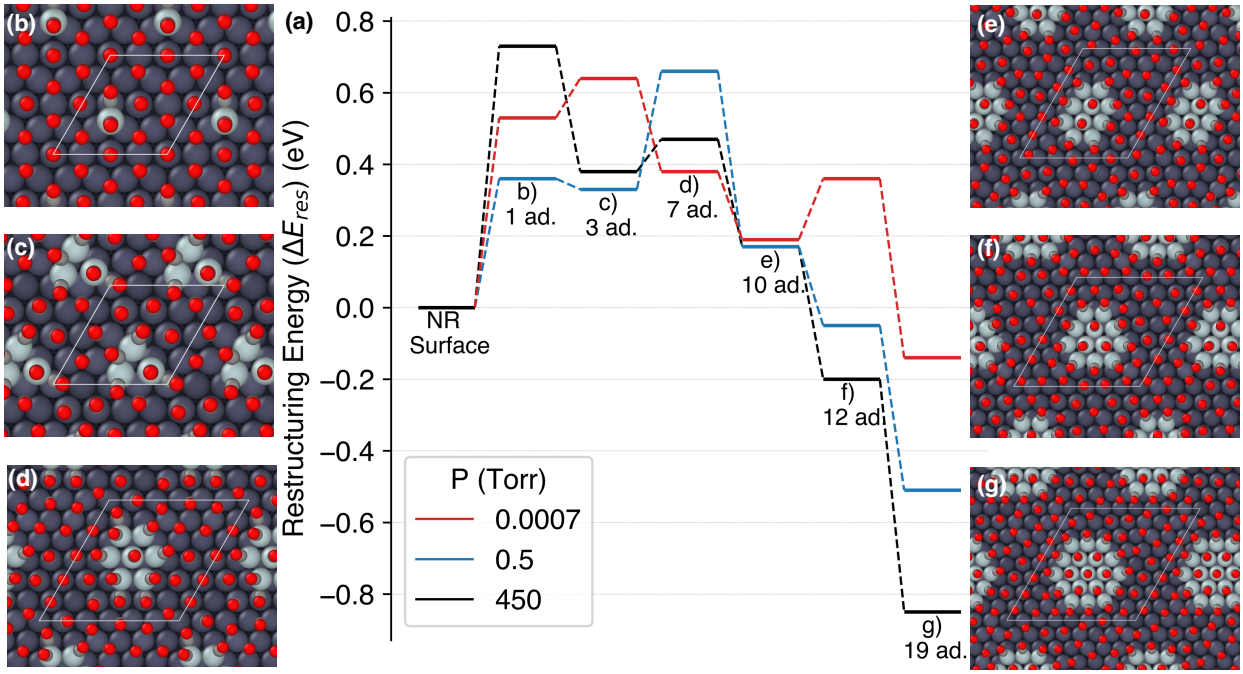

Figure 4: (a) Comparing the formation energies of Pt islands of increasing sizes from 1 to 19 atoms on a Pt(111) terrace under a CO pressure of 0.007, 0.5 or 450 Torr. (b-e) show the representative structures at a CO pressure of 450 Torr.

(ΔE_{res}) starts to decrease. Notably, restructuring Pt(111) under pressure of CO to form Pt_{12} or Pt_{19} islands is found to be exothermic. Such islands are far from being stable in the absence of CO. For example, the formation energy of Pt_{19} island on a Pt(111) surface is +7 eV (+0.4 eV per Pt atom) in the absence of CO. However, compared to CO on a terrace of Pt(111) of similar size, the net gain in CO adsorption energy in the presence of the Pt_{19} island is between 7.5 and 8 eV depending on the pressure, which can compensate the energy cost of forming such islands, making these reconstructions thermodynamically favorable(see Fig. S16, S19).

3.4 Kinetics of Pt restructuring under CO pressure

Beyond thermodynamics, kinetic aspects are also crucial for our understanding of restructuring processes. Exploring of specific pathways for all these restructuring events whose thermodynamics were extensively studied here is highly challenging and beyond the scope of this report. Fig. 5 shows a representative example where CO-induced Pt mobility can occur with a moderate energy barrier when a one-Pt-atom protrusion at a Pt(553) step edge is extracted towards

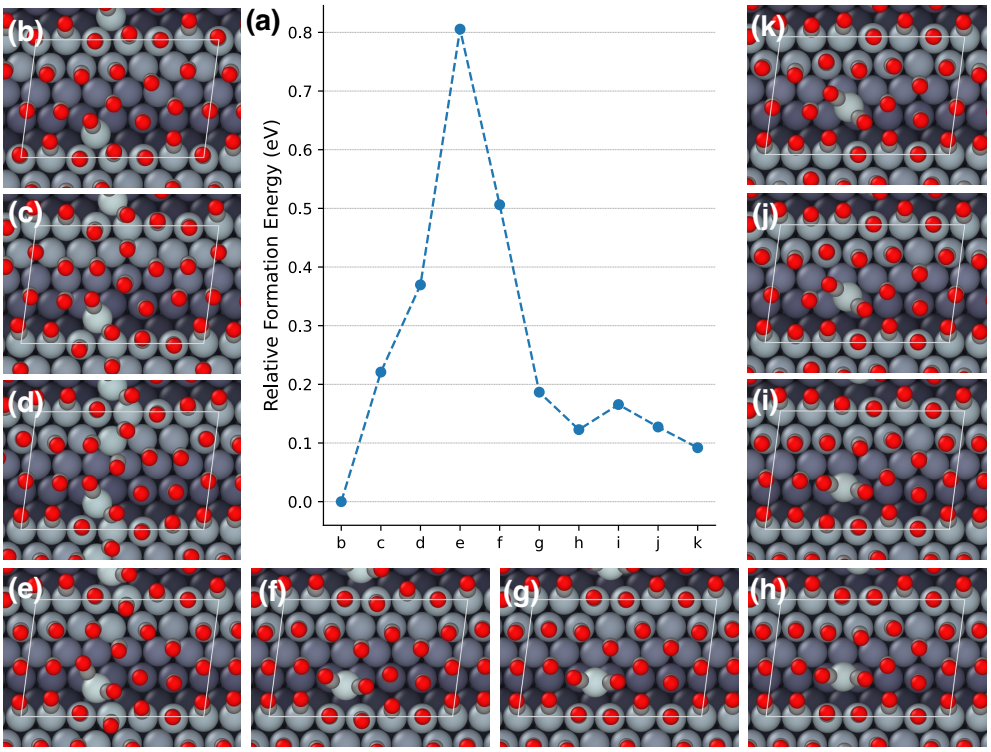

Figure 5: Kinetic reaction pathway for a restructuring event on Pt(553); (a) Reaction energy profile for the detachment of one Pt atom from the Pt(553) step edge (b-h) and its diffusion on the terrace (h-k) at a CO pressure of 450 Torr.

the terrace, while the other pathway (diffusion on the terrace) is shown in Fig. S20 (see section 2: Methods).In the initial configuration of the pathway (Fig. 5(b)), the Pt atom is attached to the step edge and, at the considered pressure condition (450 Torr) the total equilibrium CO coverage is 0.57 ML, one CO binding to the protruding Pt atom. In the final configuration (Fig. 5(k)), the Pt atom is on the terrace, stabilized by the formation of a dicarbonyl surface complex, and the equilibrium coverage of 0.6 ML (i.e. one more CO in the unit cell). The key point for a favorable energy pathway is to first rearrange the CO molecules on the initial configuration, by forming a metastable structure with one more CO adsorbate (Fig. 5(c)), less stable in free energy by 0.22 eV but with an additional CO coordination for the protruding atom, bridging with a step-edge Pt. This precursor state adopts a configuration that facilitates the detachment of the Pt atom by the formation of a dicarbonyl surface complex, with an overall energy barrier of 0.8 eV and a pathway shown from Fig.5(c) to Fig.5(h). The end of the process is simply an easy diffusion of the Pt-dicarbonyl moiety on the surface Fig.5(g-k). The fluxionality of

the CO adlayer is of crucial importance, enabling the protruding Pt atom to reach, at a modest energy cost, a configuration of CO ligands optimal for the restructuring event (Fig. 5). The calculated barrier for CO-assisted atomic extraction from the step edge is accessible at 300 K and is compatible with the experimental time scales of restructuring.

3.5 Discussion

The main qualitative reason for the restructuring is the formation of lower-coordination Pt atom sites, where CO chemisorbs more strongly, thus compensating for the energy cost arising from the restructuring of the bare surface. Since breaking the Pt-Pt bond and adsorption of CO are the main contributors with opposing consequences to the catalyst rearrangement, the restructuring energy (ΔE_{res}) can be conveniently decomposed into the energy required for breaking Pt-Pt bonds (ΔE_{metal}, positive) (on the bare surface) and the energy gained from the enhanced CO adsorption strength due to the modified coordination of Pt atoms upon restructuring, (ΔE_{chem}, negative) such that ΔE_{res} = ΔE_{metal} + ΔE_{chem}. If $|\Delta E_{chem}| \geq |\Delta E_{metal}|$, restructuring is thermodynamically favorable (Table S2, S4, S6).

When comparing the effect of the step structure, in the absence of CO adsorbates, the Pt(553) step is more difficult to restructure than Pt(557) (by 0.37-0.99 eV for Pt atoms step rearrangement and 0.19-0.71 eV for step extraction, Fig. S14). On Pt (557), the restructuring results in formation of (111) step edges, which are more stable than the initial (100) step edge, making the process energetically favorable. Unlike Pt (557), the restructuring in Pt(553) starts from a (111) step to form (100) microsteps, which are less stable (Fig. 3(d)). The restructuring energies to form small detached islands on Pt(553) (Fig. 3(i-k)) are similar to that on Pt(557). The relatively less energetically favorable restructuring on Pt(553) shows that the structure of the step is another significant descriptor for restructuring.

The investigated islands in Fig. 4 can be separated into two families. At small size (Pt_1 to Pt_7) CO can bind to the cluster through several types of modes including atop or bridge on island, atop or bridge between island and support. Starting at a size of 10 Pt atoms a more regular pattern emerges: each Pt atom is covered by one CO on the island, such a high coverage

being permitted because CO molecule can tilt outward to release the Pauli repulsion between them at a short distance (2.7-3 Å).[16] These subnanometer-size islands (Pt_{10}-Pt_{19}) combine a smaller destabilization to form the bare island (per Pt atom) and still a large fraction of low coordination edge atoms that provide stabilization from stronger CO binding. Stability of the subnano-island hence results from a subtle balance between low metal coordination and stabilization from CO adsorbates.

The correlation between restructuring energy and CO coverage is more complex than could be initially thought. Restructuring enhances CO adsorption because it creates sites with lower coordination at step/edge. Therefore, the number of CO at step/edge sites is generally increased upon restructuring. On terraces, CO adsorbates adopt a quasihexagonal arrangement[48] that develops in extended Moiré patterns on large (111) areas.[47,63] By moving Pt atoms towards the terrace, restructuring perturbs this quasihexagonal arrangement and therefore destabilizes CO adsorption on the terrace. As a result, the number of CO adsorbates on the terrace can decrease upon restructuring. This destabilization of CO on terraces is more important at high CO pressure, since the CO coverage is higher. Overall, CO adsorption is stabilized upon restructuring, but this results from a combination of stabilization at the additional low-coordinated step sites and destabilization at terraces. Therefore, a higher CO pressure does not necessarily stabilize the restructuring, as can be seen in Figs. 2, 3, and 4. Nevertheless, the formation of nano-scale islands on Fig. 4 (islands with 12 and 19 Pt atoms) is more favorable at higher pressure since their more regular shapes and CO organization disturbs less the CO packing on the terrace.

At this point we can compare the experimental and the computational data obtained in the present paper. Upon CO adsorption at stepped Pt terraces, the first process evidenced by both experiment and theory is a rearrangement of the step edges by displacement of Pt atoms, but without detachment of Pt atoms or clusters on the terraces. Straight step edges are transformed in wandering or zigzag ones. Experiments and theory agree that the stability of these rearrangements depends on the type of steps. Steps with (100) counter-step facets (as on the Pt(557) surface) provide easy (exothermic) restructuring with the formation of extensive triangular nano-shapes on the terraces and "zig-zag" step edges.[16] In contrast steps with (111) counter-step facets (as on the Pt(533) surface) are much less prone to rearrangement, because

these steps are intrinsically more stable and the rearranged structure is metastable. Our stepped Pt(111) sample (Fig. 1) shows such (111) steps, and the step wandering remains very moderate. The second process concerns the true detachment of a small Pt island from the step towards the terrace. This process requires large enough terraces. This is not the case on the Pt(557) surface and the triangular nano-shapes do not detach from the step upper-terrace. In contrast on our Pt(111) surface the step density is lower and fully detached subnanometer size islands are seen from the STM data and are calculated to be stable under a pressure of CO. Finally, the calculated barrier for detachment of a Pt atom assisted by high CO coverage is moderate (0.8 eV) which is fully compatible with the time scale of restructuring measured by the experiment. Our combined theory-experiment approach hence provides a detailed view on the possible pathways and mechanism of restructuring of stepped Pt surface under a pressure of CO.

Vibrational spectroscopy is a major method to characterize chemisorbed CO molecules. Indeed, the CO bond stretch frequency depends on the coordination of the surface Pt. For example, Avanesian et al. showed that the CO stretch frequency is lower when CO is bound to an undercoordinated Pt site representing the edges and corners of a Pt nanoparticle, compared to high coordination sites on the terraces.[36] This is explained by the fact that an undercoordinated Pt site results in a larger amount of charge transfer to the adsorbate leading to a larger shift in the vibrational frequency. In our case for the Pt_{12} islands on Pt(111) surface (Fig. 4(f)), the CO stretch frequency is in the range 2025-2035 cm^{-1} for the 12 CO molecules on the island, compared to 2060-2070 cm^{-1} for CO adsorption on the terrace (top site).[47] Interestingly, CO molecules adsorbed in the center of the subnano-island show a very similar stretch frequency than those bound to the periphery Pt atoms. Therefore, Pt coordination is an important parameter, but not the only one, and CO local coverage or tilt with respect to the facet normal could also play a role.[64]

Our study shows that restructuring of stepped areas of a Pt(111) surface occurs at room temperature with minute time scale. It initiates at steps and propagates toward terraces at least for 5-10 nm. Such a restructuring by subnano-island formation can be viewed as an atomic scale roughening of the (111) terraces and affects a small fraction of the surface atoms. Although this could have a major influence for catalytic reactivity by creating low coordination

sites, such restructuring might be difficult to follow by surface sensitive spectroscopic methods, since the signal could be dominated by non-restructured surface sites. It is pertinent to compare the situation of model single crystal surfaces studied here to that of supported Pt nanoparticles considered in the literature. Avenesian et al. considered Pt nanoparticles in the range 2 to 17 nm under a pressure of CO by TEM, IR and DFT.[36] They suggest no restructuring at 298K and showed restructuring of the (100) facets at 363K but did not evidence a change of structure on the (111) facets. The restructuring by island formation initiating at steps shown in the present paper would require large enough nanoparticles that can show steps on the (111) terraces ($\gtrsim$ 5 nm in size). Already at 298 K under CO, (111) terraces of large nanoparticles should be restructured with subnano-islands, but this could be difficult to see with the TEM and IR. Indeed, these small islands would result in small contrast change for TEM and they would lead to only small change of the fraction of under-coordinated sites, difficult to assess from the IR experiments. Therefore, the approaches on single crystal surface and nanoparticles are complementary. Different modes and scale of reconstruction can be present on different facets, and they can occur at different temperature. Besides Pt(111), restructuring has been reported on numerous metal surfaces with low Miller-index including Cu(111)[6], Au(111)[19], Au(110)[20], Co(0001)[21], Pd(111), Pd(100), hence it is significant to explore the restructuring mechanisms in terms of kinetics at atomic scale in the future.

4 Conclusion

We explored the atom-scale mechanism of the restructuring of stepped regions of Pt(111) under a pressure of CO and we show that restructuring initiates at step edge through the formation of Pt carbonyl subnano-islands on the lower terrace, based on both time-dependent HP-STM images and machine-learning enhancing computational studies. The generation of a fast machine learning potential allowed us to explore large surface unit cells with various surface models, a large number of adsorbate configurations, and complex surface restructuring processes. The integration of experimental in situ STM imaging and fast machine learning potential-based computational studies provides an atomic-scale understanding of the origin and mechanisms

of the restructuring of platinum surfaces under a pressure of CO. Here more generally, this paper demonstrates the importance of gaining atomic-scale comprehension of the dynamical transformation of metal catalyst surfaces, under a high coverage of adsorbates. The capture of such a dynamic atomic-scale picture of the ensemble of surface structures of a catalyst in a reactant gas is a clear prerequisite for an accurate determination of catalytic reaction mechanisms at a molecular level. These atomic-scale understandings of the dynamics of metal catalyst surfaces under reactant gas pressure offer insights on how to design catalyst/reactant systems that would promote such metal surface restructuring to dynamically create catalytic sites under reaction conditions leading to maximizing the activity or selectivity for the desired reaction.

Funding: This work was funded by NSF through Grants NSF-CHE-1800601 and NSF-CHE-1800577. The computer time was funded by the Extreme Science and Engineering Discovery Environment (XSEDE), which is supported by National Science Foundation grant number TG-CHE170060.[65] Specifically, it used the Bridges, Bridges-2 (Pittsburgh Supercomputing Center (PSC)), and SDSC Expanse compute systems. The STM images were collected from the high pressure scanning tunneling microscope funded by University of Notre Dame through faculty start-up fund.

Competing interest: The authors declare no competing interest.

Data and material availability: The complete data generated for this work is available at https://github.com/vsumaria/Pt_reconstruction/

Supplementary Material: Additional method details, STM images and computational data.

References

(1) Li, Y.; Kottwitz, M.; Vincent, J. L.; Enright, M. J.; Liu, Z.; Zhang, L.; Huang, J.; Senanayake, S. D.; Yang, W.-C. D.; Crozier, P. A., et al. Dynamic structure of active sites in ceria-supported Pt catalysts for the water gas shift reaction. *Nat Commun* **2021**,

12, 914.

(2) Vedrine, J. C. Revisiting active sites in heterogeneous catalysis: Their structure and their dynamic behaviour. *Appl. Catal., A* **2014**, *474*, 40–50.

(3) Vogt, C.; Weckhuysen, B. M. The concept of active site in heterogeneous catalysis. *Nat. Rev. Chem.* **2022**, *6*, 89–111.

(4) Yan, G.; Tang, Y.; Li, Y.; Li, Y.; Nguyen, L.; Sakata, T.; Higashi, K.; Tao, F. F.; Sautet, P. Reaction product-driven restructuring and assisted stabilization of a highly dispersed Rh-on-ceria catalyst. *Nat. Catal.* **2022**, *5*, 119–127.

(5) Loffreda, D.; Piccolo, L.; Sautet, P. Surface restructuring under gas pressure from first principles: A mechanism for CO-induced removal of the Au(110)-(1x2) reconstruction. *Phys Rev B* **2005**, *71*, 113414.

(6) Eren, B.; Zherebetskyy, D.; Patera, L. L.; Wu, C. H.; Bluhm, H.; Africh, C.; Wang, L.-W.; Somorjai, G. A.; Salmeron, M. Activation of Cu (111) surface by decomposition into nanoclusters driven by CO adsorption. *Science* **2016**, *351*, 475–478.

(7) Divins, N. J.; Angurell, I.; Escudero, C.; Pérez-Dieste, V.; Llorca, J. Influence of the support on surface rearrangements of bimetallic nanoparticles in real catalysts. *Science* **2014**, *346*, 620–623.

(8) Lira, E.; Merte, L.; Behafarid, F.; Ono, L.; Zhang, L.; Roldan Cuenya, B. Role and evolution of nanoparticle structure and chemical state during the oxidation of NO over size-and shape-controlled Pt/γ-Al2O3 catalysts under operando conditions. *ACS Catal.* **2014**, *4*, 1875–1884.

(9) Mistry, H.; Behafarid, F.; Bare, S. R.; Roldan Cuenya, B. Pressure-dependent effect of hydrogen adsorption on structural and electronic properties of Pt/γ-Al2O3 nanoparticles. *ChemCatChem* **2014**, *6*, 348–352.

(10) Lei, Y.; Zhao, H.; Rivas, R. D.; Lee, S.; Liu, B.; Lu, J.; Stach, E.; Winans, R. E.; Chapman, K. W.; Greeley, J. P., et al. Adsorbate-induced structural changes in 1–3 nm platinum nanoparticles. *J. Am. Chem. Soc.* **2014**, *136*, 9320–9326.

(11) Bare, S. R.; Kelly, S. D.; Ravel, B.; Greenlay, N.; King, L.; Mickelson, G. E. Characterizing industrial catalysts using in situ XAFS under identical conditions. *Phys Chem Chem Phys* **2010**, *12*, 7702–7711.

(12) Grosse, P.; Yoon, A.; Rettenmaier, C.; Herzog, A.; Chee, S. W.; Roldan Cuenya, B. Dynamic transformation of cubic copper catalysts during CO2 electroreduction and its impact on catalytic selectivity. *Nat Commun* **2021**, *12*, 6736.

(13) Tao, F.; Grass, M. E.; Zhang, Y.; Butcher, D. R.; Aksoy, F.; Aloni, S.; Altoe, V.; Alayoglu, S.; Renzas, J. R.; Tsung, C.-K., et al. Evolution of structure and chemistry of bimetallic nanoparticle catalysts under reaction conditions. *Journal of the American Chemical Society* **2010**, *132*, 8697–8703.

(14) Tao, F.; Grass, M. E.; Zhang, Y.; Butcher, D. R.; Renzas, J. R.; Liu, Z.; Chung, J. Y.; Mun, B. S.; Salmeron, M.; Somorjai, G. A. Reaction-driven restructuring of Rh-Pd and Pt-Pd core-shell nanoparticles. *Science* **2008**, *322*, 932–934.

(15) Shan, J.; Zhang, S.; Choksi, T.; Nguyen, L.; Bonifacio, C. S.; Li, Y.; Zhu, W.; Tang, Y.; Zhang, Y.; Yang, J. C., et al. Tuning catalytic performance through a single or sequential post-synthesis reaction (s) in a gas phase. *ACS Catalysis* **2017**, *7*, 191–204.

(16) Tao, F.; Dag, S.; Wang, L.-W.; Liu, Z.; Butcher, D. R.; Bluhm, H.; Salmeron, M.; Somorjai, G. A. Break-up of stepped platinum catalyst surfaces by high CO coverage. *Science* **2010**, *327*, 850–853.

(17) Zhu, Z.; Tao, F.; Zheng, F.; Chang, R.; Li, Y.; Heinke, L.; Liu, Z.; Salmeron, M.; Somorjai, G. A. Formation of nanometer-sized surface platinum oxide clusters on a stepped Pt (557) single crystal surface induced by oxygen: a high-pressure STM and ambient-pressure XPS study. *Nano letters* **2012**, *12*, 1491–1497.

(18) Nguyen, L.; Cheng, F.; Zhang, S.; Tao, F. Visualization of Surfaces of Pt and Ni Model Catalysts in Reactive Environments Using Ambient Pressure High Temperature Scanning Tunneling Microscopy and Understanding the Restructurings of Surfaces of Model Metal Catalysts under Reaction Conditions at Near Ambient Pressure. *J Phys Chem C* **2013**, *117*, 971–977.

(19) Piccolo, L.; Loffreda, D.; Aires, F. C. S.; Deranlot, C.; Jugnet, Y.; Sautet, P.; Bertolini, J. The adsorption of CO on Au (1 1 1) at elevated pressures studied by STM, RAIRS and DFT calculations. *Surf Sci* **2004**, *566*, 995–1000.

(20) Jugnet, Y.; Aires, F. C. S.; Deranlot, C.; Piccolo, L.; Bertolini, J. CO chemisorption on Au (1 1 0) investigated under elevated pressures by polarized reflection absorption infrared spectroscopy and scanning tunneling microscopy. *Surf Sci* **2002**, *521*, L639–L644.

(21) Wilson, J.; de Groot, C. Atomic-scale restructuring in high-pressure catalysis. *J. Phys. Chem.* **1995**, *99*, 7860–7866.

(22) Hoogers, G.; King, D. Adsorbate-induced step-doubling reconstruction of a vicinal metal surface: oxygen on Rh $\{332\}$. *Surf Sci* **1993**, *286*, 306–316.

(23) Hahn, E.; Schief, H.; Marsico, V.; Fricke, A.; Kern, K. Orientational instability of vicinal Pt surfaces close to (111). *Phys Rev Lett* **1994**, *72*, 3378.

(24) Lang, B.; Joyner, R.; Somorjai, G. Low energy electron diffraction studies of chemisorbed gases on stepped surfaces of platinum. *Surf Sci* **1972**, *30*, 454–474.

(25) Lanzillotto, A.-M.; Bernasek, S. The sulfur induced reconstruction of the Pt (S)-[6 (111)×(100)] surface. *J. Chem. Phys.* **1986**, *84*, 3553–3558.

(26) Haase, O.; Koch, R.; Borbonus, M.; Rieder, K. Role of regular steps on the formation of missing-row reconstructions: oxygen chemisorption on Ni (771). *Phys Rev Lett* **1991**, *66*, 1725.

(27) Koch, R.; Haase, O.; Borbonus, M.; Rieder, K. Can oxygen modify step arrangements? STM and LEED investigations on Ni (771). *Surf Sci* **1992**, *272*, 17–26.

(28) Dorsett, H.; Go, E.; Reutt-Robey, J.; Bartelt, N. Oxygen-induced step ordering on Ni (119). *Surf Sci* **1995**, *342*, 261–271.

(29) Castner, D.; Somorjai, G. LEED and thermal desorption studies of small molecules (H2, O2, CO, CO2, NO, C2H4, C2H2 and C) chemisorbed on the stepped rhodium (755) and (331) surfaces. *Surf Sci* **1979**, *83*, 60–82.

(30) Walko, D.; Robinson, I. Structure of Cu (115): Clean surface and its oxygen-induced facets. *Phys Rev B* **1999**, *59*, 15446.

(31) Einstein, T.; Jung, T.; Bartelt, N.; Williams, E. D.; Rottman, C. Step doubling and related transitions on vicinal surfaces. *J. Vac. Sci. Technol. A* **1992**, *10*, 2600–2605.

(32) Pearl, T.; Darling, S.; Niu, L.; Koleske, D.; Gaspar, D.; King, S.; Sibener, S. Influence of oxygen dissolution history on reconstruction behavior of a stepped metal surface. *Chem Phys Lett* **2002**, *364*, 284–289.

(33) Zhang, Z.; Zandkarimi, B.; Alexandrova, A. N. Ensembles of metastable states govern heterogeneous catalysis on dynamic interfaces. *Accounts Chem Res* **2020**, *53*, 447–458.

(34) Sun, G.; Sautet, P. Active Site Fluxional Restructuring as a New Paradigm in Triggering Reaction Activity for Nanocluster Catalysis. *Accounts Chem Res* **2021**, *54*, 3841–3849.

(35) Vendelbo, S. a.; Elkjær, C. F.; Falsig, H.; Puspitasari, I.; Dona, P.; Mele, L.; Morana, B.; Nelissen, B.; Van Rijn, R.; Creemer, J., et al. Visualization of oscillatory behaviour of Pt nanoparticles catalysing CO oxidation. *Nature materials* **2014**, *13*, 884–890.

(36) Avanesian, T.; Dai, S.; Kale, M. J.; Graham, G. W.; Pan, X.; Christopher, P. Quantitative and atomic-scale view of CO-induced Pt nanoparticle surface reconstruction at saturation coverage via DFT calculations coupled with in situ TEM and IR. *Journal of the American Chemical Society* **2017**, *139*, 4551–4558.

(37) Tao, F. F.; Nguyen, L.; Zhang, S.; Li, Y.; Tang, Y.; Zhang, L.; Frenkel, A. I.; Xia, Y.; Salmeron, M. Formation of second-generation nanoclusters on metal nanoparticles driven by reactant gases. *Nano Letters* **2016**, *16*, 5001–5009.

(38) Behler, J. Atom-centered symmetry functions for constructing high-dimensional neural network potentials. *J. Chem. Phys.* **2011**, *134*, 074106.

(39) Behler, J.; Parrinello, M. Generalized Neural-Network Representation of High-Dimensional Potential-Energy Surfaces. *Phys. Rev. Lett.* **2007**, *98*, 146401.

(40) Gastegger, M.; Schwiedrzik, L.; Bittermann, M.; Berzsenyi, F.; Marquetand, P. wACSF—Weighted atom-centered symmetry functions as descriptors in machine learning potentials. *J. Chem. Phys.* **2018**, *148*, 241709.

(41) Singraber, A.; Morawietz, T.; Behler, J.; Dellago, C. Parallel multistream training of high-dimensional neural network potentials. *J Chem Theory Comput* **2019**, *15*, 3075–3092.

(42) Kresse, G.; Hafner, J. Ab initio molecular dynamics for liquid metals. *Physical Review B* **1993**, *47*, 558.

(43) Kresse, G.; Furthmüller, J. Efficiency of ab-initio total energy calculations for metals and semiconductors using a plane-wave basis set. *Computational materials science* **1996**, *6*, 15–50.

(44) Perdew, J. P.; Burke, K.; Ernzerhof, M. Generalized gradient approximation made simple. *Physical review letters* **1996**, *77*, 3865.

(45) Blöchl, P. E. Projector augmented-wave method. *Physical review B* **1994**, *50*, 17953.

(46) Kresse, G.; Joubert, D. From ultrasoft pseudopotentials to the projector augmented-wave method. *Physical review b* **1999**, *59*, 1758.

(47) Sumaria, V.; Nguyen, L.; Tao, F. F.; Sautet, P. Optimal packing of CO at a high coverage on Pt (100) and Pt (111) surfaces. *ACS Catalysis* **2020**, *10*, 9533–9544.

(48) Sumaria, V.; Sautet, P. CO organization at ambient pressure on stepped Pt surfaces: first principles modeling accelerated by neural networks. *Chemical science* **2021**, *12*, 15543–15555.

(49) Wales, D. J.; Doye, J. P. Global optimization by basin-hopping and the lowest energy structures of Lennard-Jones clusters containing up to 110 atoms. *The Journal of Physical Chemistry A* **1997**, *101*, 5111–5116.

(50) Henkelman, G.; Jónsson, H. Improved tangent estimate in the nudged elastic band method for finding minimum energy paths and saddle points. *The Journal of chemical physics* **2000**, *113*, 9978–9985.

(51) Henkelman, G.; Uberuaga, B. P.; Jónsson, H. A climbing image nudged elastic band method for finding saddle points and minimum energy paths. *The Journal of chemical physics* **2000**, *113*, 9901–9904.

(52) Tao, F.; Nguyen, L.; Zhang, S. Design of a new reactor-like high temperature near ambient pressure scanning tunneling microscope for catalysis studies. *Review of Scientific Instruments* **2013**, *84*, 034101.

(53) Sun, G.; Sautet, P. Metastable structures in cluster catalysis from first-principles: Structural ensemble in reaction conditions and metastability triggered reactivity. *Journal of the American Chemical Society* **2018**, *140*, 2812–2820.

(54) Sun, G.; Alexandrova, A. N.; Sautet, P. Structural rearrangements of subnanometer Cu oxide clusters govern catalytic oxidation. *ACS Catalysis* **2020**, *10*, 5309–5317.

(55) Ouyang, R.; Xie, Y.; Jiang, D.-e. Global minimization of gold clusters by combining neural network potentials and the basin-hopping method. *Nanoscale* **2015**, *7*, 14817–14821.

(56) Fung, V.; Jiang, D.-e. Exploring structural diversity and fluxionality of pt n (n= 10–13) clusters from first-principles. *The Journal of Physical Chemistry C* **2017**, *121*, 10796–10802.

(57) Wales, D. J.; Scheraga, H. A. Global optimization of clusters, crystals, and biomolecules. *Science* **1999**, *285*, 1368–1372.

(58) Klenin, K.; Strodel, B.; Wales, D. J.; Wenzel, W. Modelling proteins: Conformational sampling and reconstruction of folding kinetics. *Biochimica et Biophysica Acta (BBA)-Proteins and Proteomics* **2011**, *1814*, 977–1000.

(59) Paleico, M. L.; Behler, J. Global optimization of copper clusters at the ZnO (10 1¯ 0) surface using a DFT-based neural network potential and genetic algorithms. *The Journal of Chemical Physics* **2020**, *153*, 054704.

(60) Huang, S.-D.; Shang, C.; Zhang, X.-J.; Liu, Z.-P. Material discovery by combining stochastic surface walking global optimization with a neural network. *Chemical science* **2017**, *8*, 6327–6337.

(61) Lin, Q.; Zhang, L.; Zhang, Y.; Jiang, B. Searching configurations in uncertainty space: Active learning of high-dimensional neural network reactive potentials. *Journal of Chemical Theory and Computation* **2021**, *17*, 2691–2701.

(62) Sun, G.; Alexandrova, A. N.; Sautet, P. Pt8 cluster on alumina under a pressure of hydrogen: Support-dependent reconstruction from first-principles global optimization. *The Journal of chemical physics* **2019**, *151*, 194703.

(63) Longwitz, S. R.; Schnadt, J.; Vestergaard, E. K.; Vang, R. T.; Lægsgaard, E.; Stensgaard, I.; Brune, H.; Besenbacher, F. High-coverage structures of carbon monoxide adsorbed on Pt (111) studied by high-pressure scanning tunneling microscopy. *J Phys Chem B* **2004**, *108*, 14497–14502.

(64) Loffreda, D.; Simon, D.; Sautet, P. Dependence of stretching frequency on surface coverage and adsorbate–adsorbate interactions: a density-functional theory approach of CO on Pd (111). *Surface science* **1999**, *425*, 68–80.

(65) Towns, J.; Cockerill, T.; Dahan, M.; Foster, I.; Gaither, K.; Grimshaw, A.; Hazlewood, V.; Lathrop, S.; Lifka, D.; Peterson, G. D., et al. XSEDE: accelerating scientific discovery. *Computing in science & engineering* **2014**, *16*, 62–74.

TOC Graphic

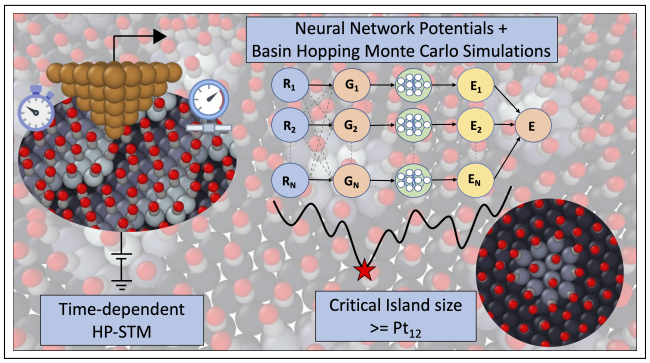
Neural Network Potentials +
Basin Hopping Monte Carlo Simulations
R1
G1
E1
R2
G2
E2
E
RN
GN
EN
Time-dependent
HP-STM
Critical Island size
>= Pt12